

Theory of magnetic anisotropy in $\text{III}_{1-x}\text{Mn}_x\text{V}$ ferromagnets

M. Abolfath,¹ T. Jungwirth,^{2,3} J. Brum,⁴ and A. H. MacDonald²

¹*Department of Physics and Astronomy, University of Oklahoma, Norman, Oklahoma 73019-0225*

²*Department of Physics, Indiana University, Bloomington, Indiana 47405*

³*Institute of Physics ASCR, Cukrovarnická 10, 162 00 Praha 6, Czech Republic*

⁴*Department of Physics, UNICAMP, Campinas, Brazil*

(Received 8 June 2000; published 8 January 2001)

We present a theory of magnetic anisotropy in $\text{III}_{1-x}\text{Mn}_x\text{V}$ -diluted magnetic semiconductors with carrier-induced ferromagnetism. The theory is based on four- and six-band envelope function models for the valence-band holes and a mean-field treatment of their exchange interactions with Mn^{++} ions. We find that easy-axis reorientations can occur as a function of temperature, carrier density p , and strain. The magnetic anisotropy in strain-free samples is predicted to have a $p^{5/3}$ hole-density dependence at small p , a p^{-1} dependence at large p , and remarkably large values at intermediate densities. An explicit expression, valid at small p , is given for the uniaxial contribution to the magnetic anisotropy due to unrelaxed epitaxial growth lattice-matching strains. Results of our numerical simulations are in agreement with magnetic anisotropy measurements on samples with both compressive and tensile strains. We predict that decreasing the hole density in current samples will lower the ferromagnetic transition temperature, but will increase the magnetic anisotropy energy and the coercivity.

DOI: 10.1103/PhysRevB.63.054418

PACS number(s): 75.50.Pp, 75.30.Gw, 73.61.Ey

I. INTRODUCTION

The discovery of carrier-mediated ferromagnetism¹⁻³ in $\text{III}_{1-x}\text{Mn}_x\text{V}$ and doped⁴ $\text{II}_{1-x}\text{Mn}_x\text{VI}$ -diluted magnetic semiconductors (DMS's) has opened up a broad and relatively unexplored frontier for both basic and applied research. Experiments^{2,5} in $\text{Ga}_{1-x}\text{Mn}_x\text{As}$ and $\text{In}_{1-x}\text{Mn}_x\text{As}$ have demonstrated that these ferromagnets have remarkably square hysteresis loops with coercivities typically ~ 40 Oe, and that the magnetic easy axis is dependent on epitaxial growth lattice-matching strains. In this paper we discuss the magnetic anisotropy properties of $\text{III}_{1-x}\text{Mn}_x\text{V}$ DMS ferromagnets, predicted by a mean-field theory⁶ of the exchange interaction coupling between localized magnetic ions and valence band free carriers. We use phenomenological four- or six-band envelope function models, depending on the carrier density p , in which the valence-band holes are characterized by Luttinger, spin-orbit splitting, and strain-energy parameters.

The physical origin of the anisotropy energy in our model is spin-orbit coupling in the valence band. Our work is based in part on theoretical descriptions developed by Gaj *et al.*⁷ and Bastard *et al.*⁸ to explain the optical properties of undoped, paramagnetic DMS's. As the critical temperature is approached, the mean-field theory we employ⁶ reduces to an earlier theory⁴ that invokes generalized RKKY carrier-mediated interactions between localized spins. The two approaches differ, however, in their description of the magnetically ordered state. As this work was nearing completion, we learned of a closely related study^{9,10} that uses the same mean-field theory to address critical temperature trends in this material class and that also addresses magnetic anisotropy physics. We are aware of three elements of the physics of these materials that make the predictions of our mean-field theory uncertain: (i) we do not account for the substantial disorder that is usually present in these ferromagnets; (ii) we

do not include effects due to interactions among the itinerant holes, and (iii) we do not account for correlations between localized spin configurations and itinerant hole states. The importance of each of these deficiencies is difficult to judge in general, and probably depends on adjustable material parameters. In our view, it is likely that there is a substantial range in the parameter space of interest where the predictions of the present theory are useful. We expect that important progress can be made by comparing this simplest possible theory of carrier-induced DMS ferromagnetism with experiment.

This work has two objectives. Most importantly, we have attempted to shed light on how various adjustable material parameters can influence magnetic anisotropy. Second, we have made an effort to estimate the magnetic anisotropy energy in those cases where experimental information is presently available. Our hope here is to initiate a process of careful and quantitative comparison between mean-field theory and experiment, partially to help judge the efficiency of this approximation in predicting other physical properties. Even in the mean-field theory, we find that the magnetic anisotropy physics of these materials is rich. We predict easy-axis reorientations as a function of hole density, exchange interaction strength, temperature, and strain and identify situations under which $\text{III}_{1-x}\text{Mn}_x\text{V}$ ferromagnets are remarkably hard.

In Sec. II we detail our mean-field theory of the ordered state. The theory simplifies in the limit of low-temperature and low-hole densities. Our results for this limit, presented in Sec. III, predict a $\langle 111 \rangle$ easy axis in the absence of strain, and a magnetic anisotropy energy that is approximately 10% of the free-carrier band-energy density. This value is extremely large for a cubic metallic ferromagnet; typical ratios in transition metal ferromagnets are smaller than 10^{-6} , for example. The anisotropy energy in this limit varies as the free-carrier density to the $5/3$ power and is independent of

the exchange-coupling strength. Explicit results for the strain dependence of the magnetic anisotropy in the same limit are presented in Sec. IV. We find that unrelaxed lattice-matching strains due to epitaxial growth contribute a uniaxial anisotropy that favors magnetization orientation along the growth direction when the substrate lattice constant is larger than the ferromagnetic semiconductor lattice constant and an in-plane orientation in the opposite case. Unfortunately, perhaps, the simple low-density limit does not normally apply in situations where high critical temperatures are expected. The more complicated, and more widely relevant, general case is discussed in Sec. V. We find that magnetic anisotropy has a nontrivial dependence on both temperature and exchange-coupling strength and that easy-axis reversals occur, in general, as a function of either parameter. According to our theory, anisotropy energy densities comparable to those in typical metallic ferromagnets are possible when the exchange coupling is strong enough to depopulate all but one of the spin-split valence bands, even with saturation magnetization values smaller by more than an order of magnitude. In the limit of large-hole densities, we find that the anisotropy energy of strain-free samples is proportional to hole density p^{-1} and exchange coupling J_{pd}^4 . We find that in typical situations a strain e_0 of only $\sim 1\%$ is sufficient to overwhelm the cubic anisotropy of strain-free samples. We conclude in Sec. VI with a discussion of the implications of these calculations for the interpretation of present experiments, and with some suggestions for future experiments that could further test the appropriateness of the model used here.

II. FORMAL THEORY

Our theory is based on an envelope-function description of the valence-band electrons, and a spin representation for their kinetic-exchange interaction¹¹ with localized d electrons¹² on the Mn^{++} ions:

$$\mathcal{H} = \mathcal{H}_m + \mathcal{H}_b + J_{pd} \sum_{i,I} \vec{S}_I \cdot \vec{s}_i \delta(\vec{r}_i - \vec{R}_I), \quad (1)$$

where i labels a valence-band hole and I labels a magnetic ion. In Eq. (1), \mathcal{H}_m describes the coupling of magnetic ions with total spin quantum number $J=5/2$ to an external field (if one is present), \vec{S}_I is a localized spin, \vec{s}_i is a hole spin, and \mathcal{H}_b is either a four- or six-band envelope-function Hamiltonian¹³ for the valence bands. In this paper we do not consider external magnetic fields so $\mathcal{H}_m \rightarrow 0$. The four-band Kohn-Luttinger model describes only the total angular momentum $j=3/2$ bands, and is adequate when spin-orbit coupling is large and the hole density p is not too large. As discussed later, in the case of GaAs, a four-band model suffices for $p \lesssim 10^{18} \text{ cm}^{-3}$. In $\text{III}_{1-x}\text{Mn}_x\text{V}$ semiconductors, the four $j=3/2$ bands are separated by a spin-orbit splitting Δ_{so} from the two $j=1/2$ bands. In the relevant range of hole and Mn^{++} densities, no more than four bands are ever occupied. Nevertheless, mixing between $j=3/2$ and $j=1/2$ bands does occur, and it can alter the balance of delicate cancellations that often controls the net anisotropy energy. The exchange interaction between valence-band holes and localized mo-

ments is believed to be antiferromagnetic,¹¹ i.e., $J_{pd} > 0$. For GaAs, experimental estimates¹⁴⁻¹⁷ of J_{pd} fall between 0.04 eV nm^3 and 0.15 eV nm^3 , with more recent work suggesting a value toward the lower end of this range.

The form of the valence band for Bloch wave vectors near the zone center in a cubic semiconductor follows from $\mathbf{k} \cdot \mathbf{p}$ perturbation theory and symmetry considerations.¹⁸ The four-band ($j=3/2$) and six band ($j=3/2$ and $1/2$) models are known as Kohn-Luttinger Hamiltonians and their explicit form is given in the Appendix. The eigenenergies are measured down from the top of the valence band, i.e., they are hole energies. The Kohn-Luttinger Hamiltonian contains the spin-orbit splitting parameter Δ_{so} and three other phenomenological parameters, γ_1 , γ_2 , and γ_3 . These are accurately known for common semiconductors. For GaAs and InAs, the two materials in which $\text{III}_{1-x}\text{Mn}_x\text{V}$ ferromagnetism has been observed, $\Delta_{so} = 0.34 \text{ eV}$ and 0.43 eV , and $(\gamma_1, \gamma_2, \gamma_3) = (6.85, 2.1, 2.9)$ and $(19.67, 8.37, 9.29)$, respectively. Most of the specific illustrative calculations discussed below are performed with GaAs parameters.

Our calculations are based on the Kohn-Luttinger Hamiltonian and on a mean-field theory in which correlations between the local-moment configuration and the itinerant carrier system are neglected. We comment later on limits of validity of this approximation. There are a number of equivalent ways of developing this mean-field theory formally. In the following paragraphs we present a view that is convenient for discussing magnetic anisotropy.

In the absence of an external magnetic field, the partition function of our model may be expressed exactly as a weighted sum over magnetic impurity configurations specified by a localized spin quantization axis, \hat{M} , and azimuthal spin quantum numbers m_I :

$$Z = \sum_{m_I} \exp(-F_b[m_I]/k_B T), \quad (2)$$

where $F_b[m_I]$ is the valence-band-free energy for holes that experience an effective Zeeman magnetic field

$$\vec{h}(\vec{r})[m_I] = -J_{pd} \hat{M} \sum_I m_I \delta(\vec{r} - \vec{R}_I). \quad (3)$$

The mean-field theory consists of replacing $\vec{h}(\vec{r})[m_I]$ by its spatial average for each magnetic impurity configuration, thereby neglecting correlations between spin distributions in local-moment and hole subsystems. The effective Zeeman magnetic field experienced by the holes then depends only on \hat{M} , the direction of the local-moment orientation, and the mean azimuthal quantum number averaged over all local moments, M :

$$\vec{h}_{MF}(M) = J_{pd} N_{Mn} M \hat{M} \equiv h \hat{M}, \quad (4)$$

where $N_{Mn} = N_I/V$ is the number of magnetic impurities per unit volume. The mean-field partition function is

$$Z_{MF}(M) = \exp\{[N_I T s(M) - F_b(\vec{h})]/k_B T\}, \quad (5)$$

where the entropy per impurity is defined by

$$s(M) = k_B \lim_{N_I \rightarrow \infty} \frac{\ln \left[\sum_{m_I} \delta \left(\sum_I m_I - N_I M \right) \right]}{N_I}, \quad (6)$$

and $F_b(\vec{h})$ is the free energy of a system of noninteracting fermions with single-particle Hamiltonian $H_b - h\hat{M} \cdot \vec{s}$.

Following standard ‘‘large number’’ arguments, $s(M)$ is readily evaluated by considering an auxiliary system consisting of magnetic impurities coupled only to an external magnetic field H . For this model problem, a familiar exercise¹⁹ gives the result

$$M(H) = JB_J(x), \quad (7)$$

where $x = g_L \mu_B H J / k_B T$, g_L is the Landé g factor of the ion, μ_B is the electron Bohr magneton, and

$$B_J(x) = \frac{2J+1}{2J} \coth[(2J+1)x/2J] - \frac{1}{2J} \coth(x/2J) \quad (8)$$

is the Brillouin function. The Brillouin function is a one-to-one mapping between reduced fields x in the interval $[0, \infty]$ and reduced magnetizations M/J in the interval $[0, 1]$; the inverse function B_J^{-1} maps M/J to x . Since the magnetization maximizes $s(M) + g_L \mu_B H M / k_B T$,

$$\frac{ds(M)}{dM} = -g_L \mu_B H / k_B T. \quad (9)$$

Equation (9) can be used to eliminate H and arrive at the following explicit expression for $s(M)$:

$$s(M) = k_B \int_{B_J^{-1}(M/J)}^{\infty} dx x \frac{dB_J(x)}{dx}. \quad (10)$$

The entropy per impurity vanishes for $M = J = 5/2$ because there is a single configuration with $\sum_I m_I = N_I J$, and approaches $\ln(2J+1) \approx 1.79$ for $M \rightarrow 0$.

The mean polarization of the localized spins at a given temperature and for a given orientation of the local moments is determined by minimizing the mean-field free energy

$$F_{MF}(M) = -k_B T \ln Z_{MF}(M) \\ = F_b(\vec{h} = N_{Mn} J_{pd} M \hat{M}) - k_B T N_I s(M), \quad (11)$$

with respect to M . Setting the derivative to zero gives

$$\frac{ds(M)}{dM} = \frac{J_{pd}}{k_B T V} \frac{dF_b(h\hat{M})}{dh}. \quad (12)$$

Comparing with Eq. (9), it follows that $F_{MF}(M)$ is minimized by $M = JB_J(g_L \mu_B H_{\text{eff}} / k_B T) = JB_J(x_{\text{eff}})$, where

$$x_{\text{eff}} \equiv \frac{g_L \mu_B H_{\text{eff}}}{k_B T} = -\frac{J_{pd}}{V k_B T} \frac{dF_b(h\hat{M})}{dh}. \quad (13)$$

It follows that $h = N_{Mn} J_{pd} M$ is determined by solving the self-consistent equation

$$h = N_{Mn} J_{pd} JB_J[x_{\text{eff}}(h)]. \quad (14)$$

Note that

$$\frac{dF_b(h\hat{M})}{dh} = \langle \vec{S}_{tot} \cdot \hat{M} \rangle, \quad (15)$$

where S_{tot} is the total hole spin, and the angle brackets indicate a thermal average for the noninteracting valence-band system. Since the valence-band system experiences an effective Zeeman coupling with strength proportional to h and direction $-\hat{M}$, it is clear that the right-hand side of Eq. (15) is negative in sign and that its magnitude increases monotonically with h , making it easy to solve Eq. (14) numerically.

To simplify the calculations presented in subsequent sections, we take advantage of the fact that temperatures of interest are almost always considerably smaller than the itinerant carrier Fermi energy. This allows us to replace $F_b(\vec{h})$ by the ground-state energy $E_b(\vec{h})$. Then, using Eq. (13) and Eq. (11), a single calculation of $E_b(h\hat{M})$ over the range from $h=0$ to $h = N_{Mn} J_{pd} J$ may be used to determine the local-moment magnetization $M(T)$ and the free energy $F(T) = F_{MF}[M(T)]$ at all temperatures.

The mean-field theory critical temperature can be identified by linearizing the self-consistent equation at small h . We find that

$$k_B T_c(\hat{M}) = -\frac{J(J+1)}{3} \frac{N_{Mn} J_{pd}^2}{V} \left. \frac{d^2 F_b(h\hat{M})}{dh^2} \right|_{h=0}. \quad (16)$$

The second derivative of the valence-band free energy with respect to field is proportional to its Pauli spin susceptibility, which is, in turn, proportional to the valence-band density of states at the Fermi energy, and to $p^{1/3}$ at small p . In the absence of strain, it follows from cubic symmetry that the right-hand side of Eq. (16) is independent of \hat{M} . Below the critical temperature, however, the mean-field free energy does depend on \hat{M} ; this dependence is the magnetic anisotropy energy we wish to calculate. We will see that the dependence of the anisotropy energy on hole density is very different from that of the critical temperature.

III. MAGNETIC ANISOTROPY IN THE STRONG EXCHANGE COUPLING LIMIT

Our mean-field theory simplifies at low temperatures and, for the four-band model, simplifies further when h is much larger than the characteristic energy scale of occupied Kohn-Luttinger states. A convenient typical energy scale is the $h=0$ hole Fermi energy ϵ_{F0} . For a given value of $N_{Mn} J_{pd}$ the largest value of h is reached at $T=0$. Then, since H_{eff} is always nonzero, $x_{\text{eff}} \rightarrow \infty$ and the solution to the mean-field equations is $M=J$, implying that $h = N_{Mn} J_{pd} J$ for every orientation \hat{M} . At $T=0$ there is no entropic contribution to the free energy and

$$F_{MF}(T=0) = E_b(\vec{h} = N_{Mn} J_{pd} J \hat{M}). \quad (17)$$

We note in passing that the magnetization density at $T=0$ has contributions from the localized spins and the itinerant spins:

$$M_s(T=0) = 2\mu_B J N_{Mn} + \frac{\kappa}{3V} \langle \vec{S}_{tot} \cdot \hat{M} \rangle, \quad (18)$$

where κ is an additional parameter of the Luttinger model. Because of the antiferromagnetic exchange interaction, the two terms here will tend to have opposite signs with the first term, which is independent of hole density, typically very dominant. For $h \gg \epsilon_{F0}$ two further simplifications occur. When the splitting of the hole bands by the effective Zeeman coupling is sufficiently large, or the hole density p is sufficiently small, only the lowest energy hole band will be occupied. Furthermore, the effective Zeeman term will dominate the mean-field single-particle Hamiltonian and, as we detail below, the envelope-function spinor for this occupied hole state has a simple analytic expression. In this section we assume that the spin-orbit splitting energy Δ_{so} is much larger than all other energies so that we can work with a four-band model. More generally, the anisotropy will depend on h/Δ_{so} , even in the limit of small hole densities.

To judge whether or not this limit can be achieved in practice, we estimate the Fermi energy of holes using the spherical approximation²⁰ in which the doubly degenerate $h=0$ bulk heavy-hole and light-hole bands are parabolic with masses $m_h = m/(\gamma_1 - 2\bar{\gamma}) \sim 0.498m$ and $m_l = m/(\gamma_1 + 2\bar{\gamma}) \sim 0.086m$, respectively. An elementary calculation then gives

$$\epsilon_{F0} = \frac{\hbar^2}{2m} \left(\frac{3\pi^2 p}{2} \right)^{2/3} \bar{\gamma}_0, \quad (19)$$

where $n = N_h/V$ is the free-carrier density and

$$\bar{\gamma}_0 = \left[\frac{(\gamma_1 - 2\bar{\gamma})^{-3/2} + (\gamma_1 + 2\bar{\gamma})^{-3/2}}{2} \right]^{-2/3}. \quad (20)$$

For GaAs $\bar{\gamma}_0 \sim 3.05$, the Fermi energy is the same as that of a system with four identical effective mass m/γ_0 bands. Typical high- T_c Ga_{1-x}Mn_xAs ferromagnetic semiconductor samples have $p \sim 0.1 \text{ nm}^{-3}$ and $N_{Mn} \sim 1.0 \text{ nm}^{-3}$ ($x \sim 0.05$), although these parameters can presumably be varied widely. Choosing a J_{pd} value in the midrange of estimated values ($\sim 0.006 \text{ Ry nm}^3$) these parameters imply that $h \sim 0.015 \text{ Ry}$ and $\epsilon_{F0} \sim 0.01 \text{ Ry}$. h is neither large compared to ϵ_{F0} , nor small compared to Δ_{so} . Thus, the simple expressions discussed in this section are not accurate for current high- T_c systems. As our ability to engineer materials improves, it should, however, be possible to grow samples that *are* in the limit discussed here. Since h is comparable to ϵ_{F0} , we know, even before performing detailed calculations, that valence-band quasiparticle spectra in paramagnetic and ferromagnetic states will differ qualitatively.

In the large- h limit the lone occupied spinor at each wave vector \vec{k} will be the member of the $j=3/2$ manifold for which the total angular momentum is aligned in the direction $-\hat{M}$; the origin of the minus sign here is the antiferromagnetic nature of the interaction between localized spins and

hole spins. Explicit expressions for the expansion of such a spin coherent state in terms of the eigenstates of j_z are known:²¹

$$|-\hat{M}\rangle = u^3 |3/2\rangle + \sqrt{3}[u^2 v |1/2\rangle + uv^2 | -1/2\rangle] + v^3 | -3/2\rangle. \quad (21)$$

In Eq. (21) $u = -i \exp(-i\phi/2) \sin(\theta/2)$ and $v = i \exp(i\phi/2) \cos(\theta/2)$, where θ and ϕ are the spherical coordinates that specify the unit vector $-\hat{M}$. In the large h/ϵ_{F0} limit, the band term in the single-particle Hamiltonian may be treated using first-order perturbation theory. Taking the expectation value of the Kohn-Luttinger Hamiltonian in the spin coherent state, we find that

$$\epsilon(\vec{k}) = -\frac{h}{2} + \langle -\hat{M} | H_L(\vec{k}) | -\hat{M} \rangle \equiv -\frac{h}{2} + \frac{\hbar^2 k^2}{2m} \gamma(\hat{M}, \hat{k}). \quad (22)$$

The first term on the right-hand side of Eq. (22) reflects the spin coherent state property,²² $\hat{M} \cdot s | -\hat{M} \rangle = -| -\hat{M} \rangle / 2$. In Eq. (22) we have noted that for any \hat{M} and any \hat{k} , the dependence of hole energy on $k = |\vec{k}|$ is quadratic. Using this property, it follows that the Fermi energy

$$\epsilon_F(\hat{M}) = \frac{\hbar^2}{2m} (6\pi^2 p)^{2/3} \bar{\gamma}(\hat{M}), \quad (23)$$

and that the ferromagnetic ground-state energy density is

$$\frac{E_b(\vec{M})}{V} = -\frac{hp}{2} + \frac{3}{5} p \epsilon_F(\hat{M}), \quad (24)$$

where

$$\bar{\gamma}(\hat{M}) \equiv \left(\int \frac{d\hat{k}}{4\pi} [\gamma(\hat{M}, \hat{k})]^{-3/2} \right)^{-2/3}. \quad (25)$$

In analogy with the $h=0$ quantity $\bar{\gamma}_0$ defined in Eq. (20), $\bar{\gamma}(\hat{M})$ is an average of the band-energy curvature over reciprocal space directions \hat{k} , with the smaller values of $\gamma(\hat{M}, \hat{k})$ weighted more heavily. Note that the factor $3\pi^2/2$ in Eq. (19) is replaced by $6\pi^2$ in Eq. (23) because only one band is occupied in this limit, instead of the four that are occupied at $h=0$. $m/\bar{\gamma}(\hat{M})$ may be thought of as a spin-orientation-dependent effective mass, which is readily evaluated as a function of \hat{M} , given the Luttinger parameters of any material. Although the magnetic condensation energy has a term proportional to J_{pd} , only the band energy contributes to the \hat{M} dependence of the ferromagnetic ground-state energy. The magnetic anisotropy energy in this limit is independent of J_{pd} and proportional to the hole density p to the 5/3 power.

We have evaluated $\gamma(\hat{M})$ as a function of angle for the Luttinger parameters of GaAs and InAs. As discussed in more detail later, we always find that magnetic anisotropy in the absence of strain is well described by a cubic harmonic expansion truncated at sixth order, an approximation com-

TABLE I. High-symmetry direction moment-orientation-dependent average Luttinger parameters and their cubic harmonic expansions for GaAs and InAs-based $\text{III}_{1-x}\text{Mn}_x\text{V}$ ferromagnetic semiconductors. These parameters specify the $T=0$ magnetic anisotropy energy in the limit of large spin-orbit splitting and large exchange-coupling parameter (J_{pd}) or small-hole density p .

Host	$\bar{\gamma}\langle 100 \rangle$	$\bar{\gamma}\langle 110 \rangle$	$\bar{\gamma}\langle 111 \rangle$	γ_1^{ca}	γ_2^{ca}
GaAs	5.965	5.088	4.639	-3.509	-4.24
InAs	13.207	10.854	9.705	-9.412	-9.84

monly used in the literature²³ on magnetic materials. The corresponding cubic harmonic expansion for $\bar{\gamma}(\hat{M})$ is

$$\begin{aligned} \bar{\gamma}(\hat{M}) = & \bar{\gamma}\langle 100 \rangle + \gamma_1^{ca}(\hat{M}_x^2\hat{M}_y^2 + \hat{M}_y^2\hat{M}_z^2 + \hat{M}_x^2\hat{M}_z^2) \\ & + \gamma_2^{ca}\hat{M}_x^2\hat{M}_y^2\hat{M}_z^2. \end{aligned} \quad (26)$$

In our calculations we find that $\bar{\gamma}(\hat{M}) < \gamma_1$ for all directions \hat{M} . This property reflects the fact that small curvature (large Fermi wave vector) directions are weighted more highly in calculating the total hole energy. For both InAs and GaAs we find that the dominant fourth-order cubic anisotropy coefficient, $\gamma_1^{ca} < 0$, indicating *nickel-type* anisotropy with easy axes along the $\langle 111 \rangle$ cube diagonal directions. At a qualitative level, the source of the higher total hole energy when the moment orientation is along a $\langle 001 \rangle$ (cube edge) direction is easy to understand. With such a moment orientation, the occupied hole orbital has $j_z = -3/2$ and energy dispersion given by $H_{hh}(\vec{k})$ in Eq. (A9). It follows that $\gamma(\hat{M} = \langle 100 \rangle, \hat{k})$ has the relatively large value $\gamma_1 + \gamma_2$ for all orientations of \hat{k} in the \hat{x} - \hat{y} plane. These large values of $\gamma(\hat{M}, \hat{k})$ are important in the average and cause the average over \hat{k} to reach its maximum for this orientation of \hat{M} .

The cubic magnetic anisotropy energy coefficients in this limit are given by

$$K_i^{ca} = + \frac{3}{5} p \frac{\hbar^2}{2m} (6\pi^2 p)^{2/3} \gamma_i^{ca}. \quad (27)$$

Values of γ_i^{ca} for GaAs and InAs are listed in Table I. We will see later that these expressions apply up to $p \sim 10^{18} \text{ cm}^{-3}$. Inserting this value for the hole density gives coefficients $\sim 2 \text{ kJ m}^{-3}$ for GaAs host material and $\sim 4 \text{ kJ m}^{-3}$ for InAs host materials; magnetic anisotropy is twice as strong in InAs in the strain-free case. These anisotropy energy coefficients are not so much smaller than those of the cubic metallic transition metal ferromagnets, despite the much higher carrier densities in the metallic case. We will see below that the scale of the semiconductor magnetic anisotropy energy does not change as the carrier density increases from 10^{18} cm^{-3} to $\sim 10^{21} \text{ cm}^{-3}$. The relatively large anisotropy energies occur despite the fact that the saturation moments M_s of $\text{III}_{1-x}\text{Mn}_x\text{V}$ ferromagnets are more than an order of magnitude smaller than their cubic metal counterparts. It follows from these values that the magnetic hardness parameters of the $\text{III}_{1-x}\text{Mn}_x\text{V}$ ferromagnets,

$$\kappa \sim \left[\frac{K_1^{ca}}{\mu_0 M_s^2} \right]^{1/2}, \quad (28)$$

will typically be larger than 1. This is unusual in cubic materials and occurs because spin-orbit coupling has a much stronger influence on semiconductor valence bands than on transition metal d bands.

As we discuss at length in Sec. V, magnetic anisotropy does not continue to increase rapidly with hole density once two or more bands are occupied in the metallic state. In current high- T_c samples, we will find that several bands are always occupied, even at zero temperature. The simple limit discussed in this section demonstrates that anisotropy energies, $T=0$ saturation moments, and critical temperatures will have radically different dependencies on engineerable parameters.

IV. STRAIN DEPENDENCE OF MAGNETIC ANISOTROPY: LOW-HOLE DENSITY LIMIT

Because of the low solubility of Mn in III-V semiconductors, $\text{III}_{1-x}\text{Mn}_x\text{V}$ materials with x large enough to produce cooperative magnetic effects cannot be obtained by equilibrium growth. The molecular beam epitaxy (MBE) growth techniques that have been successfully developed²⁴ produce $\text{III}_{1-x}\text{Mn}_x\text{V}$ films whose lattices are locked to those of their substrates. X-ray diffraction studies³ have established that the resulting strains are not relaxed by dislocations or other defects, even for thick films. Strains in the $\text{III}_{1-x}\text{Mn}_x\text{V}$ film break the cubic symmetry assumed in the previous section. Fortunately, the influence of MBE growth lattice-matching strains on the hole bands of cubic semiconductors is well understood.^{18,25} For the $\langle 001 \rangle$ growth direction used to create $\text{III}_{1-x}\text{Mn}_x\text{V}$ films, strain generates a purely diagonal contribution to the four-band single-particle envelope-function Hamiltonian in the representation we use in this paper, adding contributions $\delta\epsilon_h$ and $\delta\epsilon_l$, respectively, to $j_z = \pm 3/2$ heavy-hole and $j_z = \pm 1/2$ light-hole entries. The energy shifts are related to the lattice strains by¹⁸

$$\delta\epsilon_h = \frac{e_0}{C_{11}} \left[-2a_1(C_{11} - C_{12}) - \frac{a_2}{2}(C_{11} + 2C_{12}) \right], \quad (29)$$

$$\delta\epsilon_l = \frac{e_0}{C_{11}} \left[-2a_1(C_{11} - C_{12}) + \frac{a_2}{2}(C_{11} + 2C_{12}) \right], \quad (30)$$

where e_0 is the in-plane strain produced by the substrate-film lattice mismatch:

$$e_0 = \frac{a_S - a_F}{a_F}. \quad (31)$$

In Eqs. (29)–(31), the C_{ij} are the elastic constants of the unstrained $\text{III}_{1-x}\text{Mn}_x\text{V}$ film, which we will assume to be identical to those of the host III-V material, a_S is the lattice constant of the substrate on which the $\text{III}_{1-x}\text{Mn}_x\text{V}$ film is grown, a_F is the unstrained lattice constant of bulk $\text{III}_{1-x}\text{Mn}_x\text{V}$, and a_1 and a_2 are phenomenological deformation potentials whose values for common III-V semiconduc-

tors are known. For the six-band model the strain Hamiltonian includes off-diagonal elements and is given up to a constant times the unit matrix by

$$H_{strain} = \Gamma e_0 \begin{pmatrix} 0 & 0 & 0 & 0 & 0 & 0 \\ 0 & 1 & 0 & 0 & 0 & \frac{1}{\sqrt{2}} \\ 0 & 0 & 1 & 0 & -\frac{1}{\sqrt{2}} & 0 \\ 0 & 0 & 0 & 0 & 0 & 0 \\ 0 & 0 & -\frac{1}{\sqrt{2}} & 0 & \frac{1}{2} & 0 \\ 0 & \frac{1}{\sqrt{2}} & 0 & 0 & 0 & \frac{1}{2} \end{pmatrix}, \quad (32)$$

where $\Gamma = (\epsilon_l - \epsilon_h)/e_0 = a_2(C_{11} + 2C_{12})/C_{11}$. For GaAs and InAs, $\Gamma = -0.2382$ Ry and -0.2762 Ry, respectively.¹⁸

As in the previous section, we can derive an explicit expression for the strain contribution to the magnetic anisotropy energy when $h \gg \epsilon_{F0}$ and $h \gg \Gamma$, allowing band and strain terms to be treated as a perturbative correction to the effective Zeeman coupling, and $h \ll \Delta_{so}$, allowing a four-band model to be used. In this way we obtain

$$\frac{E_{strain}(\hat{M})}{V} = \frac{p}{4} [3\delta\epsilon_h + \delta\epsilon_l] + \frac{3p\cos^2\theta}{4} [\delta\epsilon_h - \delta\epsilon_l]. \quad (33)$$

Strain produces a uniaxial contribution to the magnetic anisotropy of $\text{III}_{1-x}\text{Mn}_x\text{V}$ films that favors orientations along the growth direction when strain shifts heavy holes down relative to the light holes and orientations in the plane in the opposite circumstance. Using Eq. (29) and Eq. (30) and deformation potential elastic constant values,¹⁸ we find that a contribution to the energy density given by $K_{strain}\sin^2(\theta)$, where the uniaxial anisotropy constant is $K_{strain} = -0.36$ Ry e_0p for GaAs and $K_{strain} = -0.41$ Ry e_0p for InAs. Since $a_2 < 0$, compressive strain ($e_0 < 0$) lowers the heavy-hole energy relative to the light-hole energy and favors moment orientations in the growth direction, while tensile strain ($e_0 > 0$) favors moment orientations perpendicular to the growth direction. Since the lattice constant of $\text{Ga}_{1-x}\text{Mn}_x\text{As}$ is larger² than that of GaAs, while that of $\text{In}_{1-x}\text{Mn}_x\text{As}$ is smaller than that of InAs, $\text{Ga}_{1-x}\text{Mn}_x\text{As}$ on GaAs is under compressive strain and $\text{In}_{1-x}\text{Mn}_x\text{As}$ on InAs is under tensile strain. Assuming³ Vergard's law, $e_0 = 0.0004$ and $e_0 = -0.0028$ for InAs and GaAs, respectively, at $x = 0.05$. For $p = 10^{-3}$ nm⁻³, a density for which this low-density result is still reasonably reliable, we find that $K_{strain} = -0.36$ kJ m⁻³ for InAs and $K_{strain} = 2.2$ kJ m⁻³ for GaAs. At these densities, strain and cubic band contributions are comparable in GaAs, but the latter contribution is dominant in the InAs case.

Strain-induced anisotropy energies can be modified by growing the magnetic film on relaxed buffer layers. This effect has been demonstrated²⁶ by Ohno *et al.* who showed that the easy axis for $\text{Ga}_{1-x}\text{Mn}_x\text{As}$ films changes from in plane to growth direction when the substrate is changed from GaAs to relaxed (In,Ga)As buffer layers. For 15% In, the magnetic film strain changes from compressive $e_0 = -0.0028$ to tensile $e_0 = 0.0077$ when this change is made. We note that the sense of this change is opposite to that predicted by our large h , small p analytic result which predicts that compressive strains favor growth direction orientations. Similarly, $\text{In}_{1-x}\text{Mn}_x\text{As}$ on InAs is under a small tensile strain but is observed to have a growth direction easy axis. (Recall that in the large- h limit the band anisotropy makes the growth direction the hard axis.) This distinction may be taken as an experimental proof that several hole bands are occupied in the magnetic ground state of these materials. The strain anisotropy energy *does* change sign at smaller values of h partly because the first band to be depopulated has primarily heavy-hole character. We will see in the next section that the mean field does predict the correct sign for the strain anisotropy energy at experimental hole densities. We conclude from the present considerations that strain can play a strong role in band-structure engineering of $\text{III}_{1-x}\text{Mn}_x\text{V}$ ferromagnet magnetic properties.

V. PARTIALLY POLARIZED HOLE BAND STATES: MAGNETIC ANISOTROPY IN THE GENERAL CASE

The results for $F_b(h\hat{M})$ discussed in the previous section become accurate when the effective Zeeman coupling h is large enough to reduce the number of occupied hole bands to one, *and* the Fermi energy remains safely smaller than the spin-orbit splitting. The situation is much more complicated at smaller h and larger hole densities. Then several bands are occupied, even at $T=0$, and these usually give competing contributions to the magnetic anisotropy. It is *not* true in general that band and strain contributions to the magnetic anisotropy are simply additive. We expect that it will eventually be possible to realize a broad range of material parameters, and hence a broad range of h values, in $\text{III}_{1-x}\text{Mn}_x\text{V}$ ferromagnets. The range of possibilities is immense, and accurate modeling of a particular sample will require accurate values for p , J_{pd} , and N_{Mn} for that material.

In this section we discuss a series of illustrative calculations, starting with ones performed using a four-band model of strain-free $\text{Ga}_{1-x}\text{Mn}_x\text{As}$ at hole density $p = 0.1$ nm⁻³. The valence-band energy density is

$$\frac{E_b}{V} = \frac{1}{V} \sum_{\mathbf{k}} \sum_{j=1}^{N_b} \theta(\epsilon_F - \epsilon_j(\mathbf{k}, \vec{h})) \epsilon_j(\mathbf{k}, \vec{h}), \quad (34)$$

where ϵ_F is the Fermi energy, \vec{k} is the Bloch wave vector, and the mean-field-theory quasiparticle energies $\epsilon_j(\mathbf{k}, \vec{h})$ are eigenvalues of the $N_b \times N_b$ single-particle Hamiltonian (N_b is the number of bands included in the envelope-function Hamiltonian)

$$H_b = H_L + \vec{h} \cdot \vec{s} + H_{strain}. \quad (35)$$

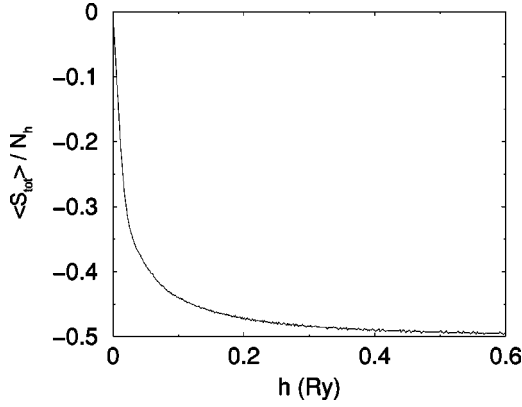


FIG. 1. Valence-band spin per hole as a function of effective Zeeman field strength h .

For a strain-free model we set $H_{\text{strain}}=0$. In Fig. 1 we plot the calculated spin polarization per hole as a function of h for a growth direction field orientation; recall that this quantity can be obtained by differentiating the energy per hole with respect to h and that the effective field seen by the localized spins is obtained by multiplying this quantity by $J_{pd}p$. The hole spin polarization increases linearly at small h with a slope proportional to the valence-band Pauli susceptibility. We see that for the hole density of Fig. 1, complete hole spin polarization is approached only at values of h comparable to or larger than the spin-orbit splitting of GaAs, so that the four-band model is not physical in this regime. For any given model, and a given moment orientation, a *single* calculation of this type provides all the microscopic information required to solve the mean-field equations at all temperatures.

For fixed values of J_{pd} , N_{Mn} , and p , h must be evaluated as a function of temperature by solving the self-consistent mean-field equation, Eq. (14), and using numerical results like those plotted in Fig. 1. For $J_{pd}=0.15 \text{ eV nm}^3$, $N_{Mn}=1 \text{ nm}^{-3}$, and $p=0.1 \text{ nm}^{-3}$ the critical temperature T_c [$h(T)=0$ for $T>T_c$] is $\sim 100 \text{ K}$, in rough agreement with experiment. There are, however, other choices of parameters that are also consistent with the measured critical temperature. In addition, as we discuss further in the next section, it is not clear that this level of theory should always yield accurate results for T_c .

At $T=0$, h reaches its maximum value, $J_{pd}N_{Mn}J \sim 0.0275 \text{ Ry}$. The dependence of energy on magnetization orientation at this value of h is illustrated in Fig. 2 and compared with the cubic harmonic expansion truncated at sixth order. The coefficients of this expansion are fixed by energy per volume calculations in $\langle 100 \rangle$, $\langle 110 \rangle$, and $\langle 111 \rangle$ directions. In Fig. 2, and in all other cases we have checked, the truncated cubic harmonic expansion is very accurate. It is therefore sufficient to evaluate the energy per volume in the high-symmetry directions and to use

$$K_1^{ca} = \frac{4(E_b\langle 110 \rangle - E_b\langle 100 \rangle)}{V}$$

$$K_2^{ca} = \frac{27E_b\langle 111 \rangle - 36E_b\langle 110 \rangle + 9E_b\langle 100 \rangle}{V}. \quad (36)$$

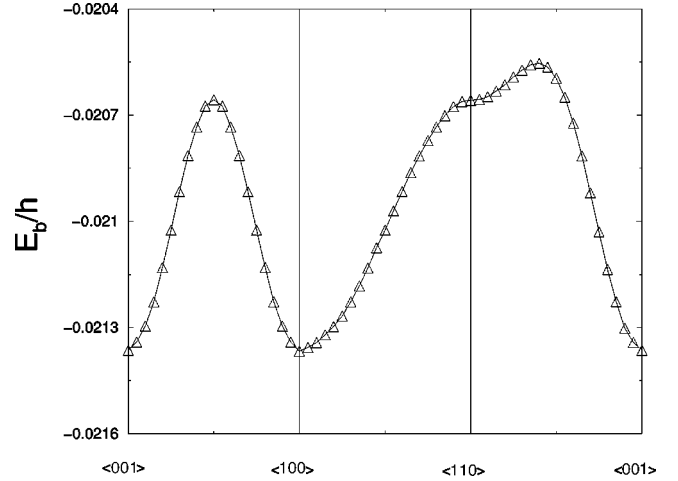


FIG. 2. Hole energy per particle in units of h as a function of magnetization orientation for $h=0.0275 \text{ Ry}$. The solid line is a cubic harmonic expansion fit to these results truncated at sixth order. At this value of h , three hole bands are partly occupied and the easy axes are the cube edge directions.

Results for $K_i^{ca}(h)$ obtained for the four-band model in this way are summarized in Fig. 3. These results can be combined with the calculated temperature dependence of the effective Zeeman coupling to obtain the model's cubic anisotropy coefficients as a function of temperature, hole density, and h . Here we see explicitly the anisotropy reversals that commonly accompany hole band depopulations. We note in Fig. 3 that the analytic results of Sec. III are recovered only for very large values of h at this density.

The valence-band Fermi surfaces of $\text{III}_{1-x}\text{Mn}_x\text{V}$ ferromagnets will be strongly dependent on both temperature and moment direction orientation. Four-band model Fermi surface intersections with the $k_z=0$ plane are illustrated in Figs. 4 and 5 for $p=0.1 \text{ nm}^{-3}$ at $h=0$ and $h=0.01 \text{ Ry}$, respectively. Both figures are for moments oriented in the $\langle 100 \rangle$ direction. The $h=0.01 \text{ Ry}$ value is the $T=0$ effective field ($J_{pd}N_{Mn}J$) for $x=0.05$ and J_{pd} at the low end of literature estimates. ($J_{pd}=0.05 \text{ eV nm}^3$.) These two figures represent the mean-field-theory Fermi surfaces at two different temperatures. In the spherical approximation, the $h=0$ Fermi

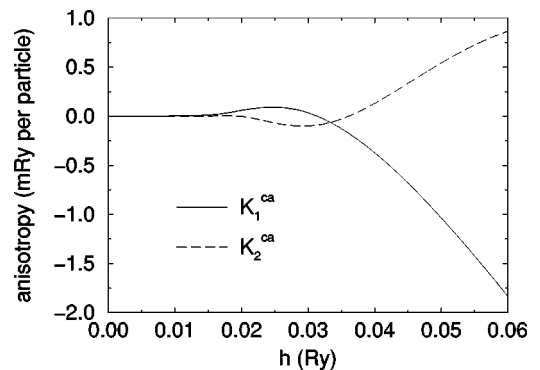


FIG. 3. The dependence of the crystalline anisotropy coefficients, $K_1^{ca}(h)$ and $K_2^{ca}(h)$ on h for a four-band model with $p=0.1 \text{ nm}^{-3}$.

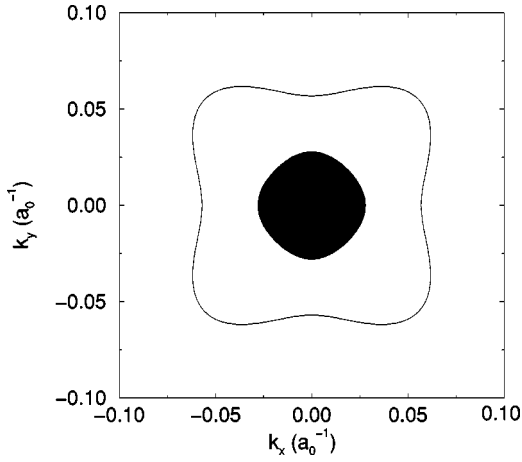


FIG. 4. Fermi surface intersection with the $k_z=0$ plane for a four-band model with $p=0.1 \text{ nm}^{-3}$ and $h=0$. Doubly degenerate heavy-hole (larger contour) and light-hole (smaller contour) bands are occupied.

energy at this hole density is $\epsilon_{F0} \sim 0.01 \text{ Ry}$, so a strong distortion of the bands is expected in the magnetic state. At $h=0$, the hole bands occur in degenerate pairs; we refer to the two less dispersive bands that occupy the larger area in \hat{k} space as heavy-hole bands, although this terminology lacks precise meaning in the general case. As h increases, both heavy- and light-hole bands split. For small h , the minority-spin heavy-hole band occupation decreases rapidly and all other band occupations increase. The heavy-hole minority-spin band is completely depopulated for $h \sim 0.04 \text{ Ry}$. Once this band is empty, the light-hole minority-spin Fermi radii begin to shrink rapidly. At still stronger fields, the majority-spin light-hole band is depopulated and the single-band limit addressed in preceding sections is achieved. For p

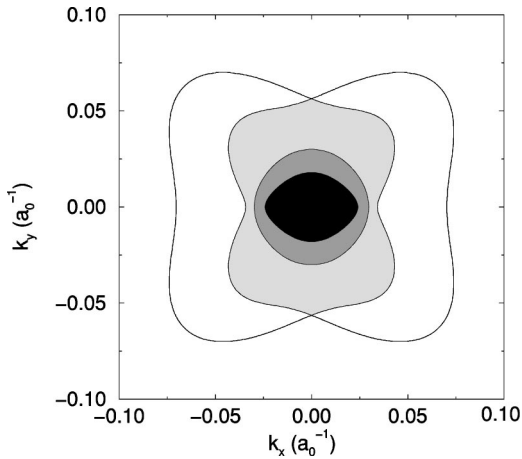


FIG. 5. Intersection of the Fermi surface and the $k_z=0$ plane for a four-band model with $p=0.1 \text{ nm}^{-3}$ and $h=0.01 \text{ Ry}$. This value of h solves the mean-field equations at $T=0$, $N_{Mn}=1 \text{ nm}^{-3}$, and $J_{pd}=0.05 \text{ eV nm}^3$, which is near the lower experimental estimate¹⁷ for the exchange coupling constant. (For $J_{pd}=0.15 \text{ eV nm}^3$ this value of h solves the mean-field equations at $T=85 \text{ K}$). The magnetization orientation is along the $\langle 100 \rangle$ direction. Heavy-hole and light-hole bands are split at nonzero h .

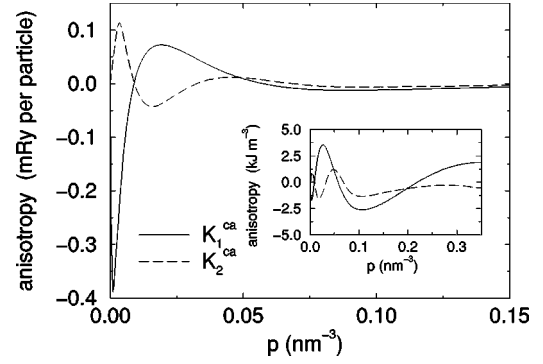


FIG. 6. Six-band model, $h=0.01 \text{ Ry}$, results for the cubic magnetic anisotropy coefficients in units of Rydberg per particle (main plot) and in kJ m^{-3} (inset).

$=0.1 \text{ nm}^{-3}$, the single-band limit is achieved only at h values for which the four-band model breaks down.

Finally, we turn to a series of illustrative calculations intended to closely model the ground state of $\text{Ga}_{0.95}\text{Mn}_{0.05}\text{As}$. For this Mn density and the smaller values of J_{pd} favored by recent estimates, $h(T=0)=J_{pd}N_{Mn}J \sim 0.01 \text{ Ry}$. This value of h is not so much smaller than the spin-orbit splitting parameter in GaAs ($\Delta_{so}=0.025 \text{ Ry}$), so that accurate calculations require a six-band model. Even with x fixed, our calculations show that the magnetic anisotropy of $\text{Ga}_{0.95}\text{Mn}_{0.05}\text{As}$ ferromagnets is strongly dependent on both hole density and strain. The hole density can be varied by changing growth conditions or by adding other dopants to the material, and strain in a $\text{Ga}_{0.95}\text{Mn}_{0.05}\text{As}$ film can be altered by changing substrates as discussed previously. The cubic anisotropy coefficients (in units of energy per volume) for strain-free material are plotted as a function of hole density in the inset of Fig. 6; the main plot shows the coefficients in units of energy per particle. Over the density range $p < 0.05 \text{ nm}^{-3}$, four- and six-band models are in good agreement. We see from this result that the asymptotic low-density region where the anisotropy energy varies as $p^{5/3}$ holds only for $p < 0.005 \text{ nm}^{-3}$ at this value of h . The easy axis is nearly always determined by the leading cubic anisotropy coefficient K_1^{ca} , except near values of p where this coefficient vanishes. As a consequence the easy axis in strain-free samples is almost always either along one of the cube edge directions ($K_1^{ca} > 0$), or along one of the cube diagonal directions ($K_1^{ca} < 0$). Transitions in which the easy axis moves between these two directions occur twice over the range of hole densities studied. (Similar transitions occur as a function of h , and therefore temperature, for fixed hole density.) Near the hole density 0.01 nm^{-3} , both anisotropy coefficients vanish and a fine-tuned isotropy is achieved. The slopes of the anisotropy coefficient curves vary as the number of occupied bands increases from 1 to 4 with increasing hole density.

Six-band model Fermi surfaces are illustrated in Figs. 7 and 8 by plotting their intersections with the $k_z=0$ plane at $p=0.1 \text{ nm}^{-3}$ for the cases of $\langle 100 \rangle$ - and $\langle 110 \rangle$ -ordered moment orientations. Comparing Fig. 5 and Fig. 7, which differ only in the band model employed, we see that there is a

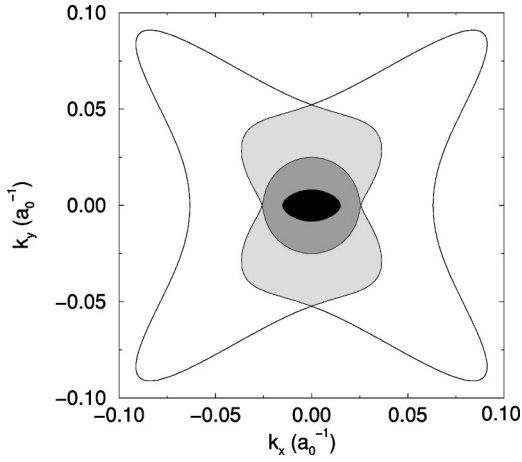


FIG. 7. Six-band model Fermi surface intersections with the $k_z=0$ plane for $p=0.1 \text{ nm}^{-3}$ and $h=0.01 \text{ Ry}$. This figure for magnetization orientation is along the $\langle 100 \rangle$ direction.

marked difference between the majority-spin heavy-hole bands in four- and six-band cases. For the six-band model, quasiparticle dispersion is particularly slow, leading to large Fermi radii along the $\langle 110 \rangle$ directions. The large and more anisotropic mass is a consequence of mixing with the split-off hole bands. This effect occurs for all ordered moment orientations, although the details of the small minority band Fermi surface projections change markedly. The dependence of quasiparticle band structure on ordered moment orientation, apparent in comparing these figures, should lead to large anisotropic magnetoresistance effects in $\text{III}_{1-x}\text{Mn}_x\text{V}$ ferromagnets. We also note that in the case of cube edge orientations, the Fermi surfaces of different bands intersect. This property could have important implications for the decay of long-wavelength collective modes.²⁷

In Fig. 9 we present mean-field theory predictions for the strain dependence of the anisotropy energy at $h=0.01 \text{ Ry}$ and hole density $p=0.35 \text{ nm}^{-3}$. According to our calculations, the easy axes in the absence of strain are along the cube edges in this case. This calculation is thus for a hole

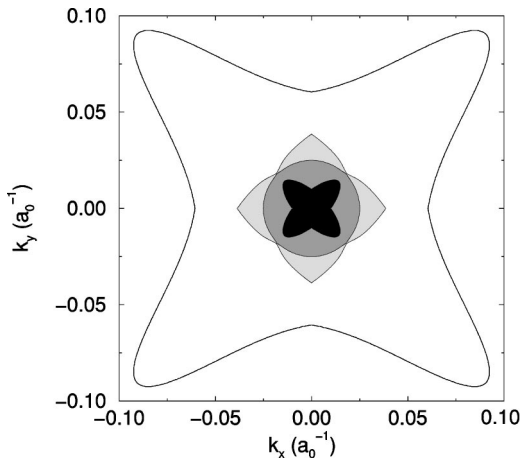


FIG. 8. Six-band model Fermi surface intersections with the $k_z=0$ plane for the parameters of Fig. 7 and magnetization orientation along the $\langle 110 \rangle$ direction.

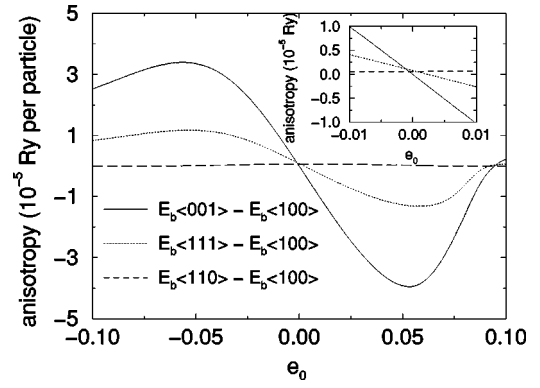


FIG. 9. Energy differences among $\langle 001 \rangle$, $\langle 100 \rangle$, $\langle 110 \rangle$, and $\langle 111 \rangle$ magnetization orientations versus in-plane strain e_0 at $h=0.01 \text{ Ry}$ and $p=0.35 \text{ nm}^{-3}$. For compressive strains ($e_0 < 0$) the system has an easy magnetic plane perpendicular to the growth direction. For tensile strains ($e_0 > 0$) the anisotropy is easy axis with the preferred magnetization orientation along the growth direction. The anisotropy changes sign at large tensile strain.

density approximately three times smaller than the Mn density, as indicated by recent experiments. The relevant value of e_0 depends on the substrate on which the epitaxial $\text{Ga}_{0.95}\text{Mn}_{0.05}\text{As}$ film is grown, as discussed in Sec. IV. The most important conclusion from Fig. 9 is that strains as small as 1% are sufficient to completely alter the magnetic anisotropy energy landscape. For example, for $(\text{Ga},\text{Mn})\text{As}$ on GaAs , $e_0 = -0.0028$ at $x=0.05$, the anisotropy has a relatively strong uniaxial contribution even for this relatively modest compressive strain, which favors in-plane moment orientations, in agreement with experiment. A relatively small ($\sim 1 \text{ kJ m}^{-3}$) residual plane anisotropy remains that favors $\langle 110 \rangle$ over $\langle 100 \rangle$. For $x=0.05$ $(\text{Ga}, \text{Mn})\text{As}$ on a $x=0.15$ $(\text{In}, \text{Ga})\text{As}$ buffer the strain is tensile, $e_0=0.0077$, and we predict a substantial uniaxial contribution to the anisotropy energy that favors growth direction orientations, again in agreement with experiment. For the tensile case, the anisotropy energy changes more dramatically than for compressive strains due to the depopulation of higher subbands, as shown in Fig. 10. At large tensile strains, the sign of the anisotropy changes emphasizing the subtlety of these effects and the latitude that exists for strain engineering of magnetic properties.

VI. DISCUSSION

We first comment on the implications of the considerations described in this paper for the interpretation of current experiments. The hysteretic effects that reflect magnetic anisotropy have been studied most extensively for the highest T_c samples currently available. These mean-field-theory predictions depend on three phenomenological parameters; N_{Mn} , which is sample dependent but accurately known; J_{pd} , which should be nearly universal for a given III-V host compound but is less accurately known; and the hole density p , which is sample dependent and not accurately known. Values of J_{pd} and p must be inferred from experiment, sometimes by comparison with theoretical pictures that are not yet

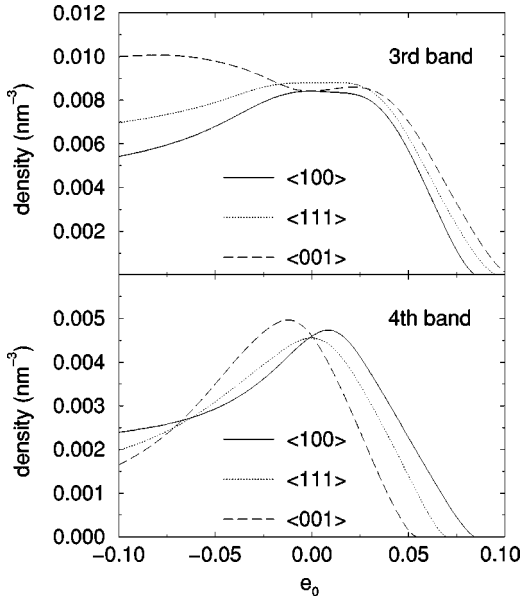


FIG. 10. Third and fourth-band densities for $\langle 100 \rangle$, $\langle 111 \rangle$, and $\langle 001 \rangle$ magnetization orientations versus in-plane strain e_0 at $h = 0.01$ Ry and $p = 0.35$ nm $^{-3}$. Curves for the $\langle 110 \rangle$ magnetization orientation (not shown here) are similar to those for the $\langle 100 \rangle$ orientation.

fully developed. The reliability of J_{pd} and p estimates is improving and presumably will continue to improve. It now seems clear that the values of J_{pd} and p in current high- T_c samples are such that several hole bands are partially occupied in the ferromagnetic ground state. In this case, we see from Fig. 3 that our calculations predict cube edge easy axes that include the growth direction. The anisotropy energies are typically $\sim 10^{-6}$ Ry nm $^{-3} \sim 1$ kJ m $^{-3}$. Similar anisotropy energies are produced by strains as small as $e_0 \sim 0.001$ and more typical strains produce larger anisotropy energies. An important conclusion from this work is that strain contributions to the anisotropy will not normally be negligible.

We believe that the in-plane easy axis observed in Ga $_{1-x}$ Mn $_x$ As films grown on GaAs is a consequence of compressive strain in the magnetic film that dominates the cubic band anisotropy energy. When Ga $_{1-x}$ Mn $_x$ As is grown on (In, Ga)As, the lattice-matching strain is tensile, reinforcing the growth direction easy-axis anisotropy of strain-free samples. (As discussed earlier, the signs of both strain and cubic band contributions to strain change when the light-hole bands are depopulated.) We note that in our calculations, the cubic band anisotropy is almost always dominated by the fourth cubic harmonic coefficient. Given this, it follows that only the cube edge easy axes that includes the growth direction axis, and cube diagonal axes that are not in the film plane, are possible without strain.

Since the local moments are fully polarized in the ferromagnetic ground state, it is easy to estimate the saturation moment $M_s \sim N_{Mn} g_L \mu_B J$, leading to the relatively small numerical value $\mu_0 M_s \sim 0.05$ T. It follows that the growth direction orientation magnetostatic energy, $\sim \mu_0 M_s^2 \sim 0.1$ kJ m $^{-3}$, is considerably smaller than the magnetocryst-

alline anisotropy coefficient. Even when several hole bands are occupied with competing spin-orbit interactions, these materials have relatively large magnetic hardness parameters. Unlike the case of metallic thin film ferromagnets that have much larger saturation moments, the magnetostatic *shape anisotropy* plays a minor role in the dependence of total energy on moment orientation. The small saturation moment will also tend to lead to large domain sizes and square easy-axis direction hysteresis loops, as seen in experiment.

Coercivities can be estimated²⁸ from the anisotropy fields defined by

$$\mu_0 H_a \sim \mu_0 M_s \frac{K}{\mu_0 M_s^2}. \quad (37)$$

For hard magnetic materials, anisotropy fields are much larger than saturation magnetizations. The itinerant field places an upper bound on, and is expected to scale with, the coercivity. Our calculations suggest that the coercivity in ferromagnetic samples with a single partially occupied hole band will be immensely larger than the coercivity of current samples. Such samples could be fabricated, for example, by adding donors such as Si to current samples, further compensating the Mn acceptors. According to mean-field theory, this modification in the sample preparation procedure will lower the ferromagnetic critical temperature, and, at the same time, increase the anisotropy energy.

Finally, we conclude with a few words of caution. This theory of magnetic anisotropy has three principal limitations: (i) it is based on a mean-field theory description of the exchange interaction between localized spins and valence-band holes; (ii) it neglects hole-hole interactions; and (iii) it does not account for disorder scattering of the itinerant holes. Confronting these weaknesses would in each case considerably complicate the theory, and we feel it is appropriate to seek progress by comparing the present relatively simple theory with experiment. Nevertheless, it is worthwhile to speculate on where and how the theory may be expected to fail.

Mean-field theory should be reliable when the range of the hole-mediated interaction between localized spins is long *and* the spin-stiffness parameter that characterizes the energy of long-wavelength spin fluctuations is sufficiently large. Considerations of this type suggest²⁹ that mean-field theory will fail at high temperatures unless the ratio of the hole density to the localized spin density is small and the field h is not too large compared to the Fermi energy. Since p is typically smaller than N_{Mn} because of antisite defects in low-temperature MBE growth samples, mean-field theory is likely to be reasonable at least at $T=0$ in many (III,Mn)V ferromagnets.

Hole-hole interactions will clearly tend to favor the ferromagnetic state by countering the band-energy cost of the spin polarization. Because of strong spin-orbit coupling in the valence band, estimates based on many-body calculations for electron gas systems may be of little use in estimating the importance of this effect more quantitatively. Work is currently in progress that should shed more light on this

matter.³⁰ Nevertheless, it seems likely that these interactions will not have an overriding importance, at least in large hole density samples.

Finally, we come to disorder. It is clear from experiment that disorder does not have a qualitative impact on free-carrier-mediated ferromagnetism even when those free carriers have been localized by a random disorder potential. It seems likely that disorder will destroy the ferromagnetic state only when the localization length becomes comparable to the distance between localized spins. On the other hand, since elastic disorder scattering will mix band states with different orientations on the Fermi surface, it also seems clear that a reduction in magnetic anisotropy energy must result. Indeed the coercivities that follow from our anisotropy energy results appear to be larger than what is observed. As far as we are aware, no theory of this effect exists at present.

ACKNOWLEDGMENTS

We gratefully acknowledge helpful interactions with W.A. Atkinson, T. Dietl, J. Furdyna, J.A. Gaj, J. König, B.-H. Lee, E. Miranda, Hsiu-Hau Lin, and Hideo Ohno. Work at the University of Oklahoma was supported by the NSF under Grant No. EPS-9720651 and a grant from the Oklahoma State Regents for Higher Education. Work at Indiana University was performed under NSF Grant Nos. DMR-9714055 and DGE-9902579. Work at the Institute of Physics ASCR was supported by the Grant Agency of the Czech Republic under Grant No. 202/98/0085, and by the Ministry of Education of the Czech Republic under Grant No. OC P5.10. A.H.M. gratefully acknowledges the hospitality of UNICAMP where project work was initiated.

APPENDIX

In the literature, different representations are used for the four-band and six-band model Kohn-Luttinger Hamiltonians. In the interest of completeness and clarity, this appendix specifies the expressions on which our detailed calculations are based. Detailed derivations of $\mathbf{k}\cdot\mathbf{p}$ perturbation theory for cubic semiconductors can be found elsewhere.¹⁸

The $k=0$ states at the top valence band have p -like character and can be represented by the $l=1$ orbital angular momentum eigenstates $|m_l\rangle$. In the coordinate representation we can write

$$\begin{aligned}\langle \mathbf{r} | m_l = 1 \rangle &= -\frac{1}{\sqrt{2}} f(r) (x + iy), \\ \langle \mathbf{r} | m_l = 0 \rangle &= f(r) z, \\ \langle \mathbf{r} | m_l = -1 \rangle &= \frac{1}{\sqrt{2}} f(r) (x - iy).\end{aligned}\tag{A1}$$

The Kohn-Luttinger Hamiltonian for systems with no spin-orbit coupling, \mathcal{H}_L , is written in the representation of the following combinations of $|m_l\rangle$:

$$\begin{aligned}|X\rangle &= \frac{1}{\sqrt{2}} (|m_l = -1\rangle - |m_l = 1\rangle), \\ |Y\rangle &= \frac{i}{\sqrt{2}} (|m_l = -1\rangle + |m_l = 1\rangle), \\ |Z\rangle &= |m_l = 0\rangle.\end{aligned}\tag{A2}$$

It reads

$$\mathcal{H}_L = \begin{pmatrix} Ak_x^2 + B(k_y^2 + k_z^2) & Ck_x k_y & Ck_x k_z \\ Ck_y k_x & Ak_y^2 + B(k_x^2 + k_z^2) & Ck_y k_z \\ Ck_z k_x & Ck_z k_y & Ak_z^2 + B(k_x^2 + k_y^2) \end{pmatrix},\tag{A3}$$

where

$$\begin{aligned}A &= -\frac{\hbar^2}{2m} (\gamma_1 + 4\gamma_2), \\ B &= -\frac{\hbar^2}{2m} (\gamma_1 - 2\gamma_2), \\ C &= -\frac{3\hbar^2}{m} \gamma_3,\end{aligned}\tag{A4}$$

m is the bare electron mass, and γ_1 , γ_2 , and γ_3 are the phenomenological Luttinger parameters. To include spin-orbit coupling we use the basis formed by total angular momentum eigenstates $|j, m_j\rangle$:

$$\begin{aligned}|1\rangle &\equiv |j = 3/2, m_j = 3/2\rangle, \\ |2\rangle &\equiv |j = 3/2, m_j = -1/2\rangle, \\ |3\rangle &\equiv |j = 3/2, m_j = 1/2\rangle, \\ |4\rangle &\equiv |j = 3/2, m_j = -3/2\rangle, \\ |5\rangle &\equiv |j = 1/2, m_j = 1/2\rangle, \\ |6\rangle &\equiv |j = 1/2, m_j = -1/2\rangle.\end{aligned}\tag{A5}$$

The basis (A5) is related to the orbital angular momentum ($m_l=1,0,-1$) and spin ($\sigma=\uparrow,\downarrow$) eigenstates by

$$\begin{aligned}
 |1\rangle &= |m_l=1,\uparrow\rangle, \\
 |2\rangle &= \frac{1}{\sqrt{3}}|m_l=-1,\uparrow\rangle + \sqrt{\frac{2}{3}}|m_l=0,\downarrow\rangle, \\
 |3\rangle &= \frac{1}{\sqrt{3}}|m_l=1,\downarrow\rangle + \sqrt{\frac{2}{3}}|m_l=0,\uparrow\rangle, \\
 |4\rangle &= |m_l=-1,\downarrow\rangle, \\
 |5\rangle &= -\frac{1}{\sqrt{3}}|m_l=0,\uparrow\rangle + \sqrt{\frac{2}{3}}|m_l=1,\downarrow\rangle, \\
 |6\rangle &= \frac{1}{\sqrt{3}}|m_l=0,\downarrow\rangle - \sqrt{\frac{2}{3}}|m_l=-1,\uparrow\rangle,
 \end{aligned} \tag{A6}$$

or

$$|1\rangle = -\frac{1}{\sqrt{2}}(|X,\uparrow\rangle + i|Y,\uparrow\rangle),$$

$$\begin{aligned}
 |2\rangle &= \frac{1}{\sqrt{6}}(|X,\uparrow\rangle - i|Y,\uparrow\rangle) + \sqrt{\frac{2}{3}}|Z,\downarrow\rangle, \\
 |3\rangle &= -\frac{1}{\sqrt{6}}(|X,\uparrow\rangle + i|Y,\uparrow\rangle) + \sqrt{\frac{2}{3}}|Z,\uparrow\rangle, \\
 |4\rangle &= \frac{1}{\sqrt{2}}(|X,\downarrow\rangle - i|Y,\downarrow\rangle), \\
 |5\rangle &= -\frac{1}{\sqrt{3}}(|X,\downarrow\rangle + i|Y,\downarrow\rangle) - \frac{1}{\sqrt{3}}|Z,\uparrow\rangle, \\
 |6\rangle &= -\frac{1}{\sqrt{3}}(|X,\uparrow\rangle - i|Y,\uparrow\rangle) + \frac{1}{\sqrt{3}}|Z,\downarrow\rangle.
 \end{aligned} \tag{A7}$$

The six-band model Kohn-Luttinger Hamiltonian, H_L , in the representation of vectors (A5) is

$$H_L = \begin{pmatrix} \mathcal{H}_{hh} & -c & -b & 0 & \frac{b}{\sqrt{2}} & c\sqrt{2} \\ -c^* & \mathcal{H}_{lh} & 0 & b & -\frac{b^*\sqrt{3}}{\sqrt{2}} & -d \\ -b^* & 0 & \mathcal{H}_{lh} & -c & d & -\frac{b\sqrt{3}}{\sqrt{2}} \\ 0 & b^* & -c^* & \mathcal{H}_{hh} & -c^*\sqrt{2} & \frac{b^*}{\sqrt{2}} \\ \frac{b^*}{\sqrt{2}} & -\frac{b\sqrt{3}}{\sqrt{2}} & d^* & -c\sqrt{2} & \mathcal{H}_{so} & 0 \\ c^*\sqrt{2} & -d^* & -\frac{b^*\sqrt{3}}{\sqrt{2}} & \frac{b}{\sqrt{2}} & 0 & \mathcal{H}_{so} \end{pmatrix}. \tag{A8}$$

In matrix (A8) we highlighted the four-band model Hamiltonian. The Kohn-Luttinger eigenenergies are measured down from the top of the valence band, i.e., they are hole energies and we use the following notation:

$$\mathcal{H}_{hh} = \frac{\hbar^2}{2m} [(\gamma_1 + \gamma_2)(k_x^2 + k_y^2) + (\gamma_1 - 2\gamma_2)k_z^2], \tag{A9}$$

$$\mathcal{H}_{lh} = \frac{\hbar^2}{2m} [(\gamma_1 - \gamma_2)(k_x^2 + k_y^2) + (\gamma_1 + 2\gamma_2)k_z^2],$$

$$\mathcal{H}_{so} = \frac{\hbar^2}{2m} \gamma_1 (k_x^2 + k_y^2 + k_z^2) + \Delta_{so},$$

$$b = \frac{\sqrt{3}\hbar^2}{m} \gamma_3 k_z (k_x - ik_y),$$

$$c = \frac{\sqrt{3}\hbar^2}{2m} [\gamma_2 (k_x^2 - k_y^2) - 2i\gamma_3 k_x k_y],$$

$$d = -\frac{\sqrt{2}\hbar^2}{2m} \gamma_2 [2k_z^2 - (k_x^2 + k_y^2)].$$

The four-band Kohn-Luttinger Hamiltonian can be diagonalized analytically and yields a pair of Kramers doublets with eigenenergies

$$\varepsilon_{\mathbf{k}} = \frac{H_{hh} + H_{lh}}{2} \mp \sqrt{\frac{1}{4}(H_{hh} - H_{lh})^2 + |b|^2 + |c|^2}.$$

In the spherical approximation²⁰ ($\gamma_2, \gamma_3 \rightarrow \bar{\gamma} \equiv 0.6\gamma_2 + 0.4\gamma_3$), the top of the valence band consists of two doubly degenerate parabolic bands with effective masses $m_h = m/(\gamma_1 - 2\bar{\gamma}) \sim 0.498m$ and $m_l = m/(\gamma_1 + 2\bar{\gamma}) \sim 0.086m$. (An approximation, in which the light-hole bands, which have a much smaller density of states are ignored, is adequate for some purposes.)

The four-band and six-band representations for the hole spin-operator components read

$$s_x = \begin{pmatrix} 0 & 0 & \frac{1}{2\sqrt{3}} & 0 & \frac{1}{\sqrt{6}} & 0 \\ 0 & 0 & \frac{1}{3} & \frac{1}{2\sqrt{3}} & -\frac{1}{3\sqrt{2}} & 0 \\ \frac{1}{2\sqrt{3}} & \frac{1}{3} & 0 & 0 & 0 & \frac{1}{3\sqrt{2}} \\ 0 & \frac{1}{2\sqrt{3}} & 0 & 0 & 0 & -\frac{1}{\sqrt{6}} \\ \frac{1}{\sqrt{6}} & -\frac{1}{3\sqrt{2}} & 0 & 0 & 0 & -\frac{1}{6} \\ 0 & 0 & \frac{1}{3\sqrt{2}} & -\frac{1}{\sqrt{6}} & -\frac{1}{6} & 0 \end{pmatrix} \quad (\text{A10})$$

$$s_y = i \begin{pmatrix} 0 & 0 & -\frac{1}{2\sqrt{3}} & 0 & -\frac{1}{\sqrt{6}} & 0 \\ 0 & 0 & \frac{1}{3} & -\frac{1}{2\sqrt{3}} & -\frac{1}{3\sqrt{2}} & 0 \\ \frac{1}{2\sqrt{3}} & -\frac{1}{3} & 0 & 0 & 0 & -\frac{1}{3\sqrt{2}} \\ 0 & \frac{1}{2\sqrt{3}} & 0 & 0 & 0 & -\frac{1}{\sqrt{6}} \\ \frac{1}{\sqrt{6}} & \frac{1}{3\sqrt{2}} & 0 & 0 & 0 & \frac{1}{6} \\ 0 & 0 & \frac{1}{3\sqrt{2}} & \frac{1}{\sqrt{6}} & -\frac{1}{6} & 0 \end{pmatrix}$$

$$s_z = \begin{pmatrix} \frac{1}{2} & 0 & 0 & 0 & 0 & 0 \\ 0 & -\frac{1}{6} & 0 & 0 & 0 & -\frac{\sqrt{2}}{3} \\ 0 & 0 & \frac{1}{6} & 0 & -\frac{\sqrt{2}}{3} & 0 \\ 0 & 0 & 0 & -\frac{1}{2} & 0 & 0 \\ 0 & 0 & -\frac{\sqrt{2}}{3} & 0 & -\frac{1}{6} & 0 \\ 0 & -\frac{\sqrt{2}}{3} & 0 & 0 & 0 & \frac{1}{6} \end{pmatrix}$$

- ¹H. Ohno, H. Munekata, T. Penney, S. von Molnar, and L. L. Chang, *Phys. Rev. Lett.* **68**, 2664 (1992).
²H. Ohno, A. Shen, F. Matsukura, A. Oiwa, A. Endo, S. Katsumoto, and Y. Iye, *Appl. Phys. Lett.* **69**, 363 (1996).
³For a thorough recent review, see Hideo Ohno, *J. Magn. Magn. Mater.* **200**, 110 (1999).
⁴A. Haury, R. Wasiela, A. Arnoult, J. Cibert, S. Tatarenko, T. Dietl, and Y. Merle d'Aubigné, *Phys. Rev. Lett.* **79**, 511 (1997).
⁵H. Munekata, A. Zaslavsky, P. Fumagalli, and R. J. Gambino, *Appl. Phys. Lett.* **63**, 2929 (1993).
⁶T. Jungwirth, W. A. Atkinson, B. H. Lee, and A. H. MacDonald, *Phys. Rev. B* **59**, 9818 (1999).
⁷J. A. Gaj, R. Planel, and G. Fishman, *Solid State Commun.* **29**, 435 (1979).
⁸B. Bastard, C. Rigaux, Y. Guldner, J. Mycielski, and A. Mycielski, *J. Phys. (France)* **39**, 87 (1978).
⁹T. Dietl, H. Ohno, F. Matsukura, J. Cibert, and D. Ferrand, *Science* **287**, 1019 (2000).
¹⁰T. Dietl, H. Ohno, and F. Matsukura, cond-mat/0007190 (unpub-

lished).

- ¹¹J. K. Furdyna, *J. Appl. Phys.* **64**, R29 (1988); *Semimagnetic Semiconductors and Diluted Magnetic Semiconductors*, edited by Michel Averous and Minko Balkanski (Plenum, New York, 1991); Tomasz Dietl, in *Handbook on Semiconductors* (Elsevier, Amsterdam, 1994), Chap. 17.
¹²We assume free carrier screening makes the central cell corrections required for isolated Mn acceptors in GaAs unimportant. See A. K. Bhattacharjee and C. Benoit á la Guillaume, *Solid State Commun.* **113**, 17 (2000), and work cited therein.
¹³J. M. Luttinger and W. Kohn, *Phys. Rev.* **97**, 869 (1955).
¹⁴H. Ohno, N. Akiba, F. Matsukura, A. Shen, K. Ohtani, and Y. Ohno, *Appl. Phys. Lett.* **83**, 6548 (1998).
¹⁵J. Okabayashi, A. Kimura, O. Rader, T. Mizokawa, A. Fujimori, T. Hayashi, and M. Tanaka, *Phys. Rev. B* **58**, 4211 (1998).
¹⁶F. Matsukura, H. Ohno, A. Shen, and Y. Sugawara, *Phys. Rev. B* **57**, 2037 (1998).
¹⁷T. Omiya, F. Matsukura, T. Dietl, Y. Ohno, T. Sakon, M. Motokawa, and H. Ohno, *Physica E (Amsterdam)* (to be published).

- ¹⁸See W. W. Chow and S. W. Koch, *Semiconductor-Laser Fundamentals* (Springer-Verlag, Berlin, 1999).
- ¹⁹See, for example, Neil W. Ashcroft and N. David Mermin, *Solid State Physics* (Saunders, Orlando, 1976).
- ²⁰A. Baldereschi and N. O. Lipari, *Phys. Rev. B* **8**, 2697 (1973). See also M. Altarelli and F. Bassani, in *Handbook on Semiconductors*, edited by T. S. Moss and W. Paul (North-Holland, Amsterdam, 1982), Vol. 1, Chap. 5; M. Altarelli, in *Heterojunctions and Semiconductor Superlattices*, edited by G. Allan, G. Bastard, N. Boccara, M. Lannoo, and M. Voos (Springer-Verlag, Berlin, 1985), and work cited therein.
- ²¹See, for example, Assa Auerbach, *Interacting Electrons and Quantum Magnetism* (Springer-Verlag, New York, 1994) p. 73.
- ²²See, for example, E. Merzbacher, *Quantum Mechanics* (Wiley, New York, 1970), p. 400.
- ²³See, for example, R. Skomski and J.M.D. Coey, *Permanent Magnetism* (Institute of Physics Publishing, Bristol, 1999).
- ²⁴H. Munekata, H. Ohno, S. von Molnar, A. Segmüller, L. L. Chang, and L. Esaki, *Phys. Rev. Lett.* **63**, 1849 (1989).
- ²⁵G. L. Bir and G. E. Pikus, *Symmetry and Strain-Induced Effects in Semiconductors* (Wiley, New York, 1974).
- ²⁶H. Ohno, F. Matsukura, A. Shen, Y. Sugawara, A. Oiwa, A. Endo, S. Katsumoto, and Y. Iye, in *Proceedings of the 23rd International Conference on the Physics of Semiconductors* (World Scientific, Singapore, 1996).
- ²⁷M. Abolfath and A. H. MacDonald (unpublished).
- ²⁸R. Skomski and J.M.D. Coey, *Permanent Magnetism* (IOP Publishing, Bristol, 1999).
- ²⁹J. König, Hsiu-Hau Lin, and A. H. MacDonald, *Phys. Rev. Lett.* **84**, 5628 (2000); cond-mat/0001320 (unpublished).
- ³⁰T. Jungwirth and A. H. MacDonald (unpublished).